Determining Stellar Velocity Dispersion in Active Galaxies: Is the [OIII] Width a Valid Surrogate?

A Senior Thesis
presented to
The Physics Department
California Polytechnic State University, San Luis Obispo

by
Kelsi Flatland

advised by
Dr. Vardha N. Bennert

December, 2012

Abstract

The tight empirical relation between the stellar velocity dispersion (σ_*) of the bulge and the mass of the supermassive black hole (BH) at its center indicates a close connection between galactic evolution and BH growth. The evolution of this relation with cosmic time provides valuable clues to its origin. While the mass of the BH can be easily estimated using the Doppler broadening of the Hβ emission line in type I active galactic nuclei (AGNs), measuring σ_* simultaneously is challenging, since the nuclear emission outshines the host galaxy. Thus, it is highly desirable to find an alternative way to estimate σ_*. In the literature, the width of the [OIII] emission line has been used as a surrogate, assuming that the narrow-line region follows the gravitational potential of the bulge. While the [OIII] line has the great advantage of being easily measurable in AGNs out to large redshifts, it is also known to be affected by outflows and jets. For a sample of about 100 nearby active galaxies, we determine the width of the [OIII] line using two Gaussians to exclude any outflowing component. The resulting width is compared to a single Gaussian fit and Gauss-Hermite polynomial fit, and finally to σ_* measurements previously compiled from Keck spectroscopy for the entire sample to determine the method's viability. It is found that though subtracting the wing component makes for a much better fit, there is significant scatter in each of the fits, implying no linear relation between the width of [OIII] and σ_*.

Contents

List of Figures

List of Tables

1 Introduction

Active galactic nuclei (AGNs) are among the most powerful and energetic objects in the universe. AGNs are point-like sources in the center of their host galaxy, and are extremely luminous: on the order of 10^{11} solar luminosities ($L_\odot$), which can often outshine the entire host galaxy. They exhibit an emission spectrum instead of the typical stellar absorption spectrum of the bulge. This emission comes from a surprisingly small region, hardly larger than our solar system. The reason we know it is such a small region is due to the fact that it is unresolved in any images of these galaxies, and there is short-term variability, meaning the emission of the whole region changes on short time-scales, limiting the region to a small volume due to the finite speed of light.

What could be producing such high luminosity in such a small region? If the light did come from stars, that would mean 10^{11} suns in a region about the size of our solar system: we know this would be gravitationally unstable, so it cannot be a huge number of stars. The process we observe in the region has to be a very efficient process, more so than thermonuclear fusion as in stars. The only object we know of that can be so efficient, producing such a large luminosity in such a small spatial scale, is a black hole (BH). Now one might ask how a BH can be luminous; it is not actually the BH which is emitting radiation, but the matter spiraling into it in an accretion disk that creates the huge luminosity. This idea is explored in more detail in Section 1.1 on the unified model.

There are many categories of AGNs, though it is suspected that they are all the same type of object at different stages of evolution, with different physical properties, or seen from different angles. We will be focusing specifically on Seyfert galaxies, which contain AGNs characterized by comparatively low luminosity (Peterson 1997).

1.1 The Unified Model

The current widely-accepted geometrical model for Seyfert AGNs is illustrated in Fig. (1). The central engine consists of a BH and its accretion disk. Matter spiraling in towards the BH makes up the accretion disk and emits radiation due to the viscosity of the material, and this radiation ionizes the gas in the surrounding regions. This is a very efficient process, so very little material is actually needed to fuel the AGN: on the order of two solar masses ($M_\odot$) per year for even the most luminous AGNs, which is comparable to the rate of star formation in our own Milky Way galaxy.

Surrounding the central object is a torus of dust. This torus is optically thick, meaning that if it happens to lie in our line of sight, the dust absorbs the radiation from the central object, as well as from the photoionized gas around it, obscuring them from view.

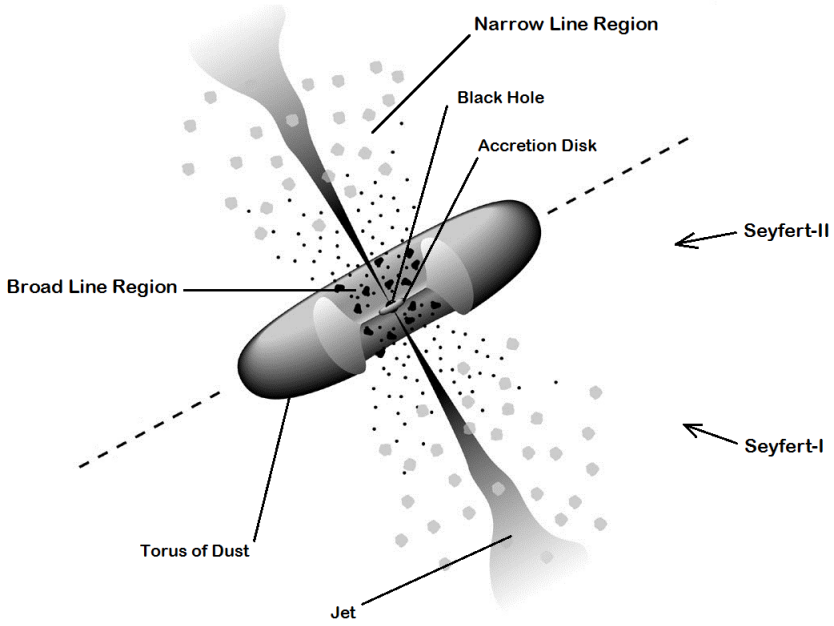

Figure 1: The geometry of an AGN. Each component is labeled, as well as the difference in viewing angles for Seyfert galaxies. Image adapted from Urry & Padovani (1995).

The dense photoionized gas in between the dusty torus and the central engine is the broad line region (BLR), and the photoionized gas extending out either end of the dusty torus is the narrow line region (NLR).

1.1.1 Broad Line Region

The BLR consists of the dense, hot gas surrounding the accretion disk in the center of the dusty torus. The mechanics in this region are governed nearly entirely by the gravitational force of the BH in the center. The photoionized gas clouds are moving around the BH at great speeds, approximately 10^3 - 10^4 km/s, causing the emission lines to be Doppler broadened due to their high velocity. This means that the emission from the material which is moving away from us at great speeds is redshifted, and the emission from the material moving towards us is blueshifted, resulting in an overall broadening of that spectral line. This broadening is attributed to the high velocity of the clouds and not the high temperature, because it is much too wide to be thermal Doppler broadening. Only certain emission lines such as the Balmer series are present and broadened in the spectra from this region.

The broadened lines of the BLR can be used to determine an important property of the central BH: the mass. The width at half maximum of the Hβ line can be used in an empirical formula to determine the mass of the BH. This equation assumes the clouds of gas are moving about the BH on Keplerian orbits due to gravitational forces, which are dominated by the BH, allowing us to use the velocity-related Doppler broadening and an estimated average radius to infer the mass of the BH.

1.1.2 Narrow Line Region

The NLR extends outside the dusty torus, and is characterized by low-density gas. Due to the opacity of the dusty torus, which blocks radiation from the central engine, we see cones of photoionized gas extending from either end of the torus, as evident in Fig. (2). The ionization cones are further evidence for the unified model. Like the BLR, the NLR is also Doppler broadened, but the velocities of the clouds in this region are much smaller, approximately 10^2 - 10^3 km/s, since they are further away from the BH. An important feature of the NLR is that it is orientation-independent: we can observe it in all objects, even if we are within the plane of the dusty torus. This contrasts the BLR, which is only visible when we are looking down the ionization cone.

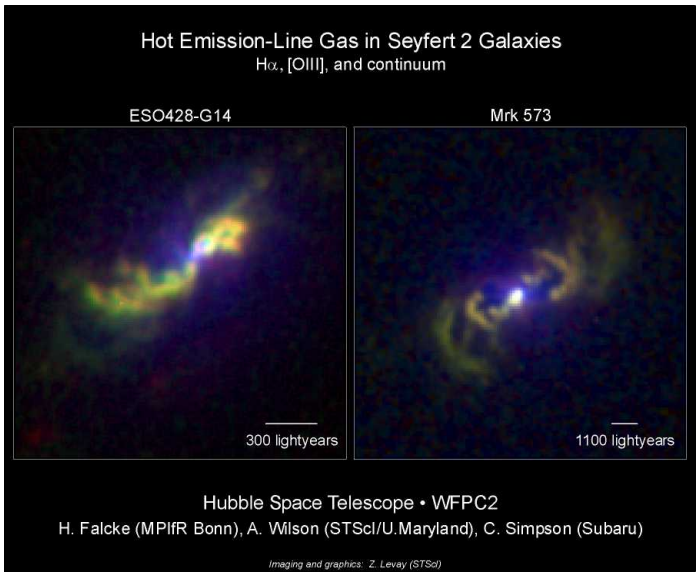

Figure 2: Two examples of ionization cones: note that the photoionized material extends on opposite sides of the central engine. Image from http://www.astro.ru.nl/~falcke/pictures.html.

Because of the lower density, forbidden transitions are prominent in the NLR, such as the

[OIII] 5007Å transition (henceforth simply referred to as [OIII]). A forbidden transition is an unlikely transition of an electron from an excited to a de-excited state; it has a very low probability of occurring due to the selection rules of quantum mechanics. Note that there are no broad forbidden lines. This is due to the higher density of the BLR, which causes the electrons of excited atoms in the region to be collisionally de-excited before the de-excitation via emission of a photon, resulting in a forbidden emission line, can occur.

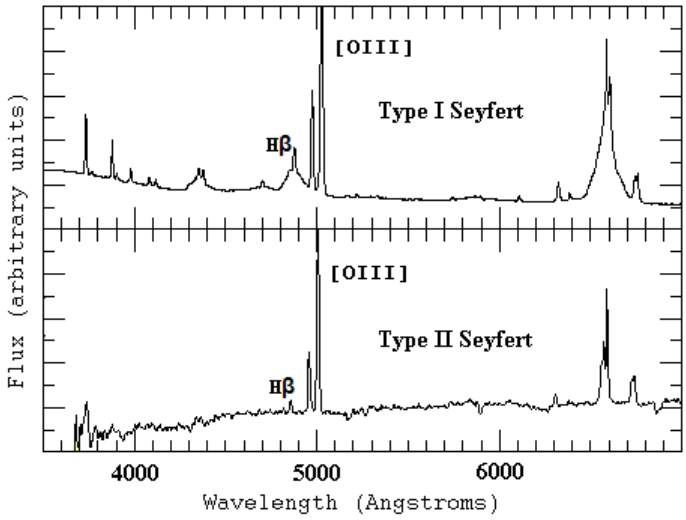

Figure 3: Sample spectra from type I and type II Seyfert galaxies. Note the Hβ has a broad component in type I, but not in type II galaxies, whereas [OIII] is narrow in both cases. Image adapted from http://www.astr.ua.edu/keel/agn/.

There are two types of Seyfert galaxies which display similar properties in their spectra, except for one dividing factor. As demonstrated in Fig. (3), both types demonstrate an emission-line spectrum, but type I Seyfert galaxies demonstrate both narrow and broad lines, while type II Seyfert galaxies have no broad lines. The mechanism behind the broadening of the lines has been explained as the Doppler broadening of the material close in by the BH. The dichotomy of Seyfert galaxies can be explained with the geometry of the AGN and its orientation with respect to us, as can be seen in Fig. (1). If we view the AGN from within the plane of the dusty torus, the dust in the torus blocks the BLR and central engine, obscuring the radiation from the inner region so we see only the NLR: this produces only narrow emission lines in the spectrum, and the galaxy is labeled as a type II Seyfert galaxy. If we view the AGN from within the cone of the NLR, the BLR is not obscured: this causes broadened emission lines to be superimposed on specific narrow lines in the spectrum, and we call it a type I Seyfert galaxy. Currently, this is the accepted model for the difference between the types of Seyfert galaxies.

Additional supporting evidence for the unified model comes in the form of polarized BLR emission detected in some type II AGNs. This emission from the otherwise obscured BLR is thought to be scattered by the electrons in the NLR into our line of sight. This suggests that the unified model is correct and that type I and type II Seyfert galaxies exhibit the same phenomenon.

1.2 Stellar Velocity Dispersion

Stellar velocity dispersion (σ_*) is a measure of the broadening of stellar absorption lines in the bulge of galaxies. It gives us an idea of how the stars in the bulge are moving around the center of the galaxy. It is basically the Doppler broadening of some stars moving towards us, some moving away, in the swarm-like movement of the stars in the bulge.

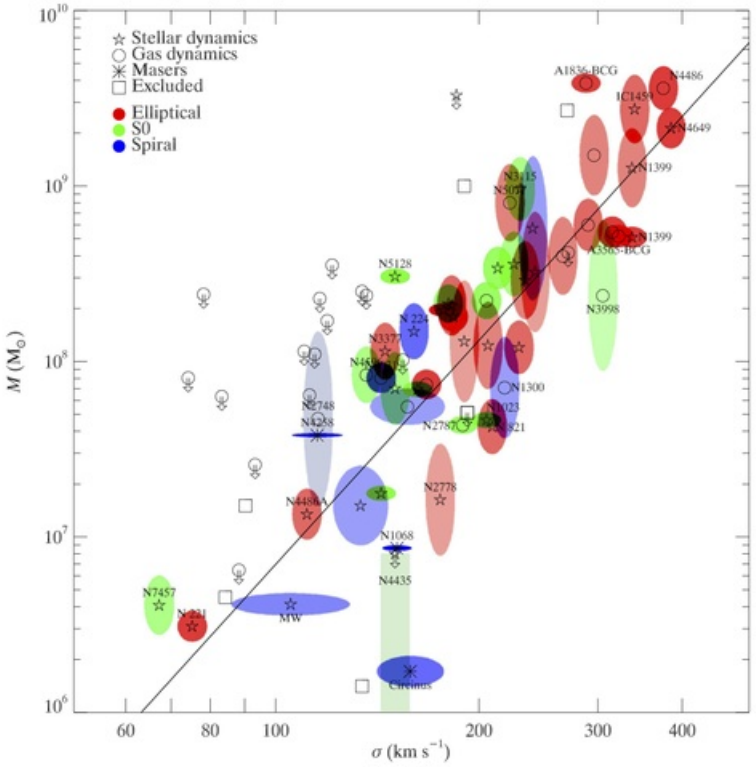

Figure 4: The relation between M_{BH} and σ_*. Figure from Gultekin et al. (2009).

An empirical relation has been found between σ_* and the mass of the BH (M_{BH}) in the center of the galaxy, as seen in Fig. (4). This is unexpected; because the BH is such a small

part of the total mass of the bulge, about 1000 times smaller in fact, the majority of the stars are not affected much by its gravitational potential. This relation is an interesting result which suggests a coevolution of BHs with their host galaxy.

However, σ_* is difficult to measure in active galaxies where the stellar spectra are outshined by the AGN. This means we are unable to observe it in many objects especially out to high redshifts, which makes high-redshift coevolution research difficult. It would be beneficial if there were some other spectral property that could be used as an alternative to σ_*.

1.3 Goal of Thesis

It has been suggested that the width of the [OIII] emission line can be used as a surrogate for σ_* since the NLR is thought to be so extended that it follows the gravitational potential of the bulge. The [OIII] line is a very prominent line in the NLR of the AGN, so it is visible out to high redshift, in any orientation of AGN, and in cases where the AGN outshines the stellar spectra. Thus it is potentially a very valuable alternative to σ_*.

There is some controversy in the literature on this subject. There are those who use the [OIII] width as a surrogate for σ_* under the assumption that the NLR follows the gravitational potential of the galactic bulge (Nelson 2000). The possibility of this correlation has been explored in papers such as Boroson et al. (2003) who concluded that there is a correlation but with a large amount of scatter.

We want to know if this surrogate is valid, so our main motivation is to see if there is a correlation between the width of the [OIII] lines and σ_*.

The [OIII] line is known to often have blue wings, which may be caused by outflow in our direction or interaction of the NLR with jets, and in any case this component does not follow the same gravitational potential as the rest of the NLR and so could affect our measurement of σ. Because of this extra component, we use several different approaches to fit the [OIII] line and compare each method (see Section 2).

We have a more extensive sample than those who have tested this before. Also, we will be taking into account the possibility of outflow components to the line, which would broaden the line and cause an overestimate of the width.

This senior thesis is organized as follows. We introduce our sample in Section 1.4. The spectral analysis is detailed in Section 2. We compare our measured $\sigma_{[OIII]}$ with σ_* in Section 3, and summarize our work and results in Section 4.

1.4 Our Sample

We have the spectra of approximately 100 local AGNs taken with the Keck-I 10m telescope from January 2009 to March 2010 (Bennert et al. 2011; Harris et al. 2012). These objects were chosen from the Sloan Digital Sky Survey (SDSS) with M_{BH} greater than 10^7 $M_\odot$, and observed with the motivation of getting a better estimate for the M_{BH}, as well as σ_*. For more information on the sample and observations, see Harris et al. (2012).

2 Spectral Analysis

The initial data processing and analysis of our sample was performed by Vardha N. Bennert and Chelsea Harris (UCSB) and has been published in Harris et al. (2012). There exist σ_* measurements for 84 objects in this sample, as has also been published in Harris et al. (2012). This senior thesis began with fully processed, de-redshifted, and normalized spectra. Several types of Python code were run on these spectra to fit the [OIII] lines. The original code was written by Matthew W. Auger (University of Cambridge, UK) and modified by Vardha N. Bennert to fit the Hβ and [OIII] region with a combination of Gaussians and Gauss-Hermite Polynomials. This code was then modified to look only at the [OIII] line with different [OIII] fitting methods by myself and Vardha N. Bennert with the assistance of Matthew W. Auger.

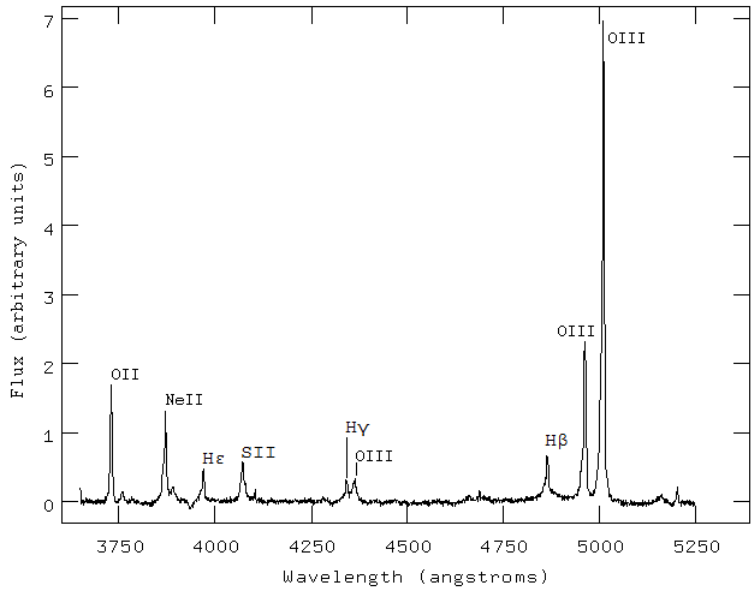

Figure 5: Sample spectrum. We are interested in the Hβ-[OIII] region: about 4750Å-5030Å.

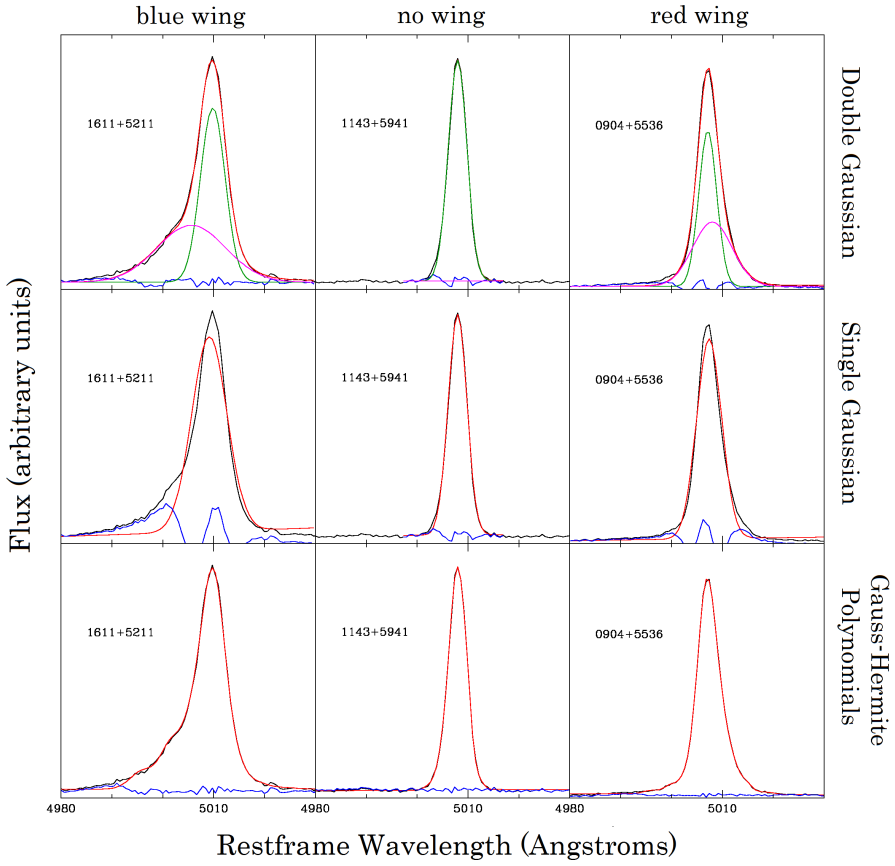

Figure 6: Samples of each fit for three objects: the first row is the double Gaussian fit, the second is the single Gaussian fit, and the third is the Gauss-Hermite polynomial fit. The first column is an object with an obvious blue wing, the middle column is an object with no obvious wing, and the last column is an object with a red wing.

2.1 Double Gaussian Fit

Our first fit is motivated by the previously stated concern that many of the [OIII] lines have a wing component, which is composed of material not following the same gravitational potential, so we only want to look at the main component of the line. We investigate using two Gaussians to fit the line: one for the main component, and one for the wing component. We then take only the width of the main component to compare to σ_*. If the [OIII] width is a valid surrogate for σ_*, we expect to see a linear relation when we plot them against each other. We expect this fit to be our best estimate of $\sigma_{[OIII]}$.

The double Gaussian code is designed to fit only the [OIII] 5007Å line with two Gaussian profiles. The entire list of objects has been run through this code, with the window size being adjusted to gain the best fit. The value of $\sigma_{[OIII]}$ is computed from the full width at half maximum (FWHM) of [OIII], which gives us an estimate of the velocity dispersion ($\sigma_{[OIII]}$) of the NLR gas in km/s. These are related by $\sigma_{[OIII]}$=FWHM/2.35 for a Gaussian. A conservative estimate for the error has been made based off the amount $\sigma_{[OIII]}$ changes due to different input parameters, such as the wavelength window.

Of the 100 objects fit with the double Gaussian code, 79 objects display a blueshifted wing, 16 have a redshifted wing, and 5 seemed to show no wing component at all. Three objects have been dropped from this fit due to a very broad Hβ line which overlapped with [OIII]. These objects are excluded from the sample for consistency, rather than including Hβ in the fit.

Appendix C contains the finalized double Gaussian fit of each object in RA+DEC order. Notice that not all of the objects needed a second Gaussian for a wing component, as the single Gaussian did a fair job on its own in a few cases. Overall though, the double Gaussian fit gave satisfying results, with small residuals.

2.2 Single Gaussian Fit

The simplest fit of [OIII] would be a single Gaussian. While the line profile of [OIII] is generally not a single Gaussian, we are merely looking for an estimate from which we can determine the width. We expect this specific fit to give us an overestimate of σ_* since it includes any wings in the line due to outflow or jet interactions, and we expect scatter when we plot this estimate against σ_*, even if $\sigma_{[OIII]}$ is a valid surrogate for σ_*, since the wings are not present in all objects.

Each object has run through this code with the same starting parameters as used in the double Gaussian fit. Again, the width of the [OIII] line was used to compute $\sigma_{[OIII]}$. The same estimate for the error was used as in the double Gaussian fit, since there were similar values and it was a conservative estimate.

2.3 Gauss-Hermite Polynomial Fit

Previous projects using this sample were motivated to measure M_{BH}, and so involved fitting the Hβ broad and narrow lines, as well as the [OIII] 5007Å and 4959Å lines in case they overlapped. The [OIII] lines were fitted with Gauss-Hermite polynomials since the

project's goal was to measure the broad Hβ line and not the [OIII] line structure. Gauss-Hermite polynomials are important because they have the ability to include asymmetries in the line profile, such as the wing component often present in [OIII] (Bennert et al. 2011). Thus this fit is our best depiction of the overall [OIII] line profile. Using the parameters from that previous project, we use this fit for an estimate of the width of the whole line, including any outflow present.

The Hβ-fitting code has been modified to output the FWHM of the [OIII] line, and each object has run through this code using the parameters previously recorded as the values for the best fit. Six objects are excluded since they had to be dropped from that project or had their own individual code, and we did not compute the [OIII] width in those cases.

All the resulting $\sigma_{[OIII]}$ measurements for the double-Gaussian fit (2G), single-Gaussian fit (1G), and the Gauss-Hermite polynomial fit (GHP) are available in Table 3, as well as the previously measured σ_* for each object.

3 Comparison with σ_*

In this section, we compare the resultant $\sigma_{[OIII]}$ estimates from each type of fit with the true σ_* from previous measurements. We have σ_* measurements for 84 objects, whereas we have $\sigma_{[OIII]}$ estimates for 100 objects with the double Gaussian fit, all 103 objects with the single Gaussian fit, and 95 objects with the Gauss-Hermite polynomial fit. Our comparison of $\sigma_{[OIII]}$ with σ_* will involve only those 75 objects which have all four values.

For the double Gaussian fit it was found that the average ratio of $\sigma_{[OIII]}/\sigma_*$ is about 0.97 with a standard deviation of 0.32. This is a significant scatter of σ values, as demonstrated in Fig. (7), which compares each $\sigma_{[OIII]}$ measurement with its corresponding σ_* value. On average, the [OIII] width gives us σ_* when using this fit, but the scatter is too large to be useful in individual cases. This is the best fit though, as a majority of the objects include outflow components. The statistics of comparing our [OIII] results to the previous measurements of σ_* for each fit may be found in Table 1.

A single Gaussian fit gave us an overestimate of σ_*, as expected. In this case the average value of $\sigma_{[OIII]}/\sigma_*$ is about 1.32 with a standard deviation of 0.51. Fig. (8) illustrates this, where we see the majority of the points are above the reference line at $\sigma_{[OIII]}/\sigma_*$=1.

The results from the Gauss-Hermite polynomial fit also turned out as expected: $\sigma_{[OIII]GHP}$ overestimated σ_*, with an average of 1.28 and a standard deviation of 0.49. This is clearly demonstrated in Fig. (9), where again most of the points lie above the reference line.

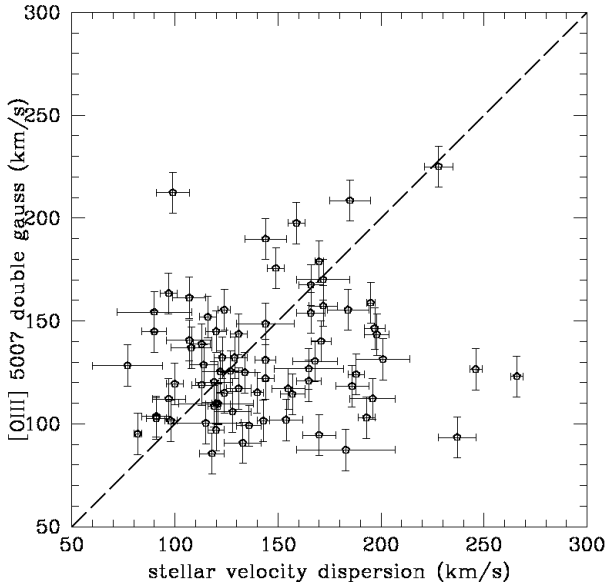

Figure 7: Double Gaussian $\sigma_{[OIII]}$ - σ_* plot. The dashed line represents $\sigma_{[OIII]}$=σ_*.

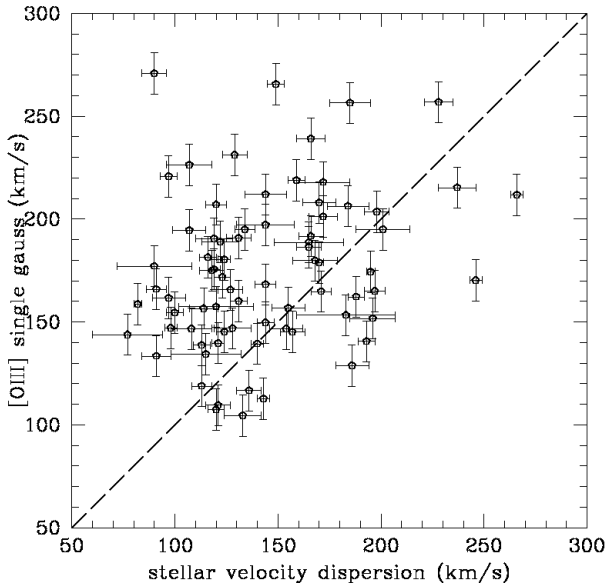

Figure 8: Single Gaussian $\sigma_{[OIII]}$ - σ_* plot. The dashed line represents $\sigma_{[OIII]}/\sigma_*$=1.

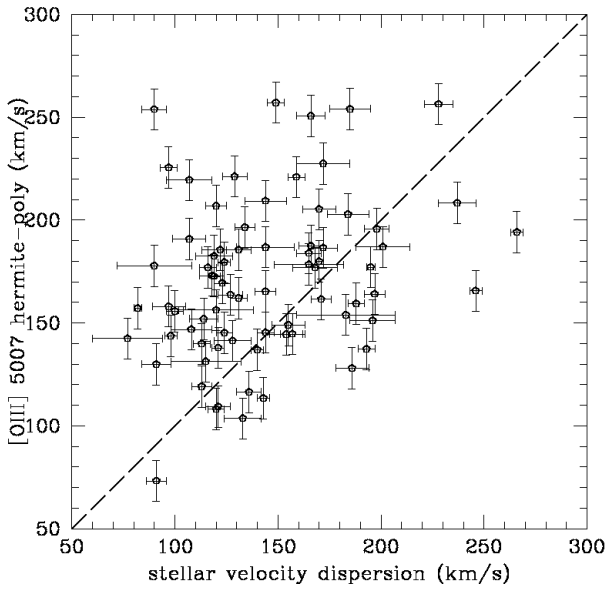

Figure 9: Gauss-Hermite polynomial $\sigma_{[OIII]}$ - σ_* plot. The dashed line represents $\sigma_{[OIII]}/\sigma_*$=1.

fit	mean	sigma	kurtosis	correlation coeff
2G	0.97	0.32	1.61	0.16
1G	1.32	0.51	8.00	0.15
GHP	1.28	0.49	7.33	0.17

Table 1: Statistics of the Three Fits

Each of the three resultant plots demonstrates significant scatter with large standard deviations, suggesting no linear relation between σ_* and $\sigma_{[OIII]}$.

4 Summary and Conclusion

The significant scatter of the σ_* vs. $\sigma_{[OIII]}$ plots suggests that there is no reliable correlation between σ_* and $\sigma_{[OIII]}$. Also, it seems that estimating the width of the [OIII] line by fitting it with two Gaussians and taking only the main line gives us the right value on average, but in individual cases can over- or underestimate σ_* by as much as a factor of three. The large scatter means the [OIII] line widths are not a valid surrogate for stellar velocity dispersion. This may render results presented for various high-redshift coevolution papers invalid.

Acknowledgments

A very special thanks to my advisor, Vardha Bennert. I would also like to acknowledge our collaborators: Tommaso Treu, Matthew Auger, and Stefanie Komossa.

References

Vardha N. Bennert, Matthew W. Auger, Tommaso Treu, Jong-Hak Woo, & Matthew A. Malkan. A Local Baseline of the Black Hole Mass Scaling Relations for Active Galaxies. I. Methodology and Results of Pilot Study. Astrophysical Journal, 726-759, Jan 2011.

T. A. Boroson, et al. Does the Narrow [OIII] λ5007 Line Reflect the Stellar Velocity Dispersion in Active Galactic Nuclei? Astrophysical Journal, 585: 647-652, Mar 2003.

Kayhan Gultekin, et al. The M-σ and M-L Relations in Galactic Bulges, and Determinations of Their Intrinsic Scatter. Astrophysical Journal, Mar 26.

Chelsea E. Harris, Vardha N. Bennert, Matthew H. Auger, Tommaso Treu, Jong-Hak Woo, & Matthew A. Malkan. A Local Baseline of the Black Hole Mass Scaling Relations for Active Galaxies. II. Measuring Stellar Velocity Dispersion in Active Galaxies. The Astrophysical Journal Supplement Series, 201-229, Aug 2012.

Charles H. Nelson. Black Hole Mass, Velocity Dispersion, and the Radio Source in Active Galactic Nuclei. Astrophysical Journal, 544: L91-L94, Dec 2000.

Bradley M. Peterson. *An Introduction to Active Galactic Nuclei.* Cambridge University Press, 1997.

C. Megan Urry, Paolo Padovani. Unified Schemes for Radio-Loud Active Galactic Nuclei. Publications of the Astronomical Society of the Pacific, 107: 803-845, Sep 1995.

Appendix A: Table of Symbols and Abbreviations

symbol/abbrev.	meaning
AGN	active galactic nucleus
BH	black hole
BLR	broad line region
FWHM	full width at half maximum
GHP	Gauss-Hermite polynomial
Hβ	Balmer series spectral line
$L_\odot$	solar luminosities
$M_\odot$	solar masses
M_{BH}	black hole mass
NLR	narrow line region
[OIII]	the [OIII] 5007Å transition
RA+DEC	right ascension & declination
SDSS	Sloan Digital Sky Survey
1G	single Gaussian
2G	double Gaussian
σ_*	stellar velocity dispersion
$\sigma_{[OIII]}$	dispersion of NLR

Table 2: Symbols and Abbreviations

Appendix B: Table of Results

The resultant $\sigma_{[OIII]}$ values from each of the three fits are listed in the table below. The σ_* values come from Harris et al. (2012).

Table 3: Results from Each Fit

object	RA+DEC	σ_{2G} [km/s]	σ_{1G} [km/s]	σ_{GHP} [km/s]	σ_* [km/s]
71	0013-0951	124.9	194.9	196.5	134
5	0026+0009	178.9	178.9	179.9	170
73	0038+0034	117.1	190.8	185.5	131
74	0109+0059	126.7	188.7	178.4	165
11	0121-0102	140.6	226.4	219.5	107
76	0150+0057	103	140.6	137.3	193
2	0206-0017	-	222	229.7	218
77	0212+1406	124.0	162.2	159.4	188
78	0301+0110	163.4	220.8	225.5	97
79	0301+0115	144.8	270.8	253.8	90
80	0310-0049	66.2	85.4	84.3	-
9	0336-0706	126.5	170.2	165.6	246
6	0353-0623	112.2	151.7	151.2	196
81	0731+4522	169.7	256.4	252.8	-
82	0735+3752	101.3	143.5	-	156
83	0737+4244	154.3	177.1	177.8	90
16	0802+3104	138.7	138.7	139.8	113
1	0802+3104	115.4	138.6	136.4	-
114	0811+1739	99.1	116.6	116.4	136
10	0813+4608	96.9	107.4	108.1	120
208	0831+0521	131.3	195	186.9	201
126	0845+3409	87.2	103.9	-	1211
4	0846+2522	-	149.9	145.6	25
8	0847+1824	-	242.6	241.5	-
130	0854+1741	135.3	312.1	314.7	-
19	0857+0528	118.9	144.3	-	127
20	0904+5536	105.8	146.9	141.3	128
21	0909+1330	102.6	165.9	73.2	91
22	0921+1017	101.5	147	143.7	98
23	0923+2254	132.2	231.2	221.2	129
138	0923+2946	101.4	112.7	113.4	143

Continued on next page

Table 3 – *Continued from previous page*

object	RA+DEC	σ_{2G} [km/s]	σ_{1G} [km/s]	σ_{GHP} [km/s]	σ_* [km/s]
24	0927+2301	158.8	174.4	177.1	195
26	0932+0233	115	145.2	145.2	124
27	0932+0405	113.9	137	-	96
143	0936+1014	214.6	251	249.5	-
28	0938+0743	155.4	180.3	179.5	124
29	0948+4030	115.1	139.4	136.9	140
30	1002+2648	101.9	146.7	144.4	154
155	1029+1408	146.4	165	164	197
31	1029+2728	125.6	165.6	163.7	127
156	1029+4019	120.8	186.4	183.9	165
157	1038+4658	111.5	135.6	131.6	-
32	1042+0414	137	146.7	146.8	108
33	1043+1105	110.1	110.1	108.4	-
34	1049+2451	128.3	143.8	142.4	77
162	1058+5259	109.8	139.7	137.9	121
35	1101+1102	148.6	197.2	186.8	144
36	1104+4334	103.6	133.4	129.8	91
37	1110+1136	103	129.7	126.7	-
13	1116+4123	143.6	160.1	162.1	131
38	1118+2827	108.5	175.6	172.6	119
14	1132+1017	168.2	198.9	196.1	-
39	1137+4826	153.9	239.1	250.6	166
174	1139+5911	103.2	130.3	116	-
40	1140+2307	95.1	158.6	157.2	82
177	1143+5941	109.5	109.5	109.3	121
15	1144+3653	117	156.8	149	155
41	1145+5547	85.5	175	173	118
180	1147+0902	109.8	157.4	156.3	120
187	1205+4959	167.5	191.7	187.4	166
42	1206+4244	114.4	145.1	144.6	157
43	1210+3820	131	168.2	165.3	144
44	1216+5049	157.3	201.2	186.5	172
45	1223+0240	112.1	161.6	158	97
210	1228+0951	155.4	206.3	202.8	184
196	1231+4504	225	256.9	256.4	228
197	1241+3722	122	149.7	145.3	144
202	1246+5134	118.8	118.8	119.1	113

Continued on next page

Table 3 – *Continued from previous page*

object	RA+DEC	σ_{2G} [km/s]	σ_{1G} [km/s]	σ_{GHP} [km/s]	σ_* [km/s]
46	1250-0249	161.3	194.6	190.8	107
47	1306+4552	119.4	154.5	155.7	100
48	1307+0952	109.9	124	126	-
204	1312+2628	90.7	104.5	103.6	133
213	1313+3653	87.3	153.3	153.9	183
49	1323+2701	125.3	189	185.5	122
207	1353+3951	130.4	179.8	176.8	168
50	1355+3834	137.7	164.2	166.3	-
51	1405-0259	132.2	171.8	169.3	123
52	1416+0137	175.6	265.6	257.1	149
53	1419+0754	208.5	256.5	254	185
209	1423+2720	90.4	121.1	-	128
54	1434+4839	128.6	156.5	151.9	114
56	1505+0342	132.1	171.8	165.5	-
57	1535+5754	151.9	181.4	176.9	116
214	1543+3631	120.3	190.5	182.5	119
58	1545+1709	140.1	164.8	161.5	171
59	1554+3238	197.6	218.9	220.9	159
60	1557+0830	116.2	139.3	139	-
61	1605+3305	118.3	128.8	128	186
62	1606+3324	94.5	208	205.3	170
63	1611+5211	144.9	207	206.9	120
205	1636+4202	189.8	212	209.3	144
64	1647+4442	100.5	115.3	-	-
88	1655+2014	196.5	260	-	199
91	1708+2153	170.1	217.9	227.4	172
96	2116+1102	123.6	234.3	205.6	-
99	2140+0025	102.5	209.9	-	71
100	2215-0036	174.7	237.4	234.6	-
102	2221-0906	100.3	134.3	131.2	115
103	2222-0819	212.4	383.3	367.3	99
106	2233+1312	143.4	203.6	195.7	198
108	2254+0046	159.8	311.2	313.9	-
70	2327+1524	123	211.8	194.1	266
109	2351+1552	93.4	215.3	208.3	237

Appendix C: Double Gaussian Fits

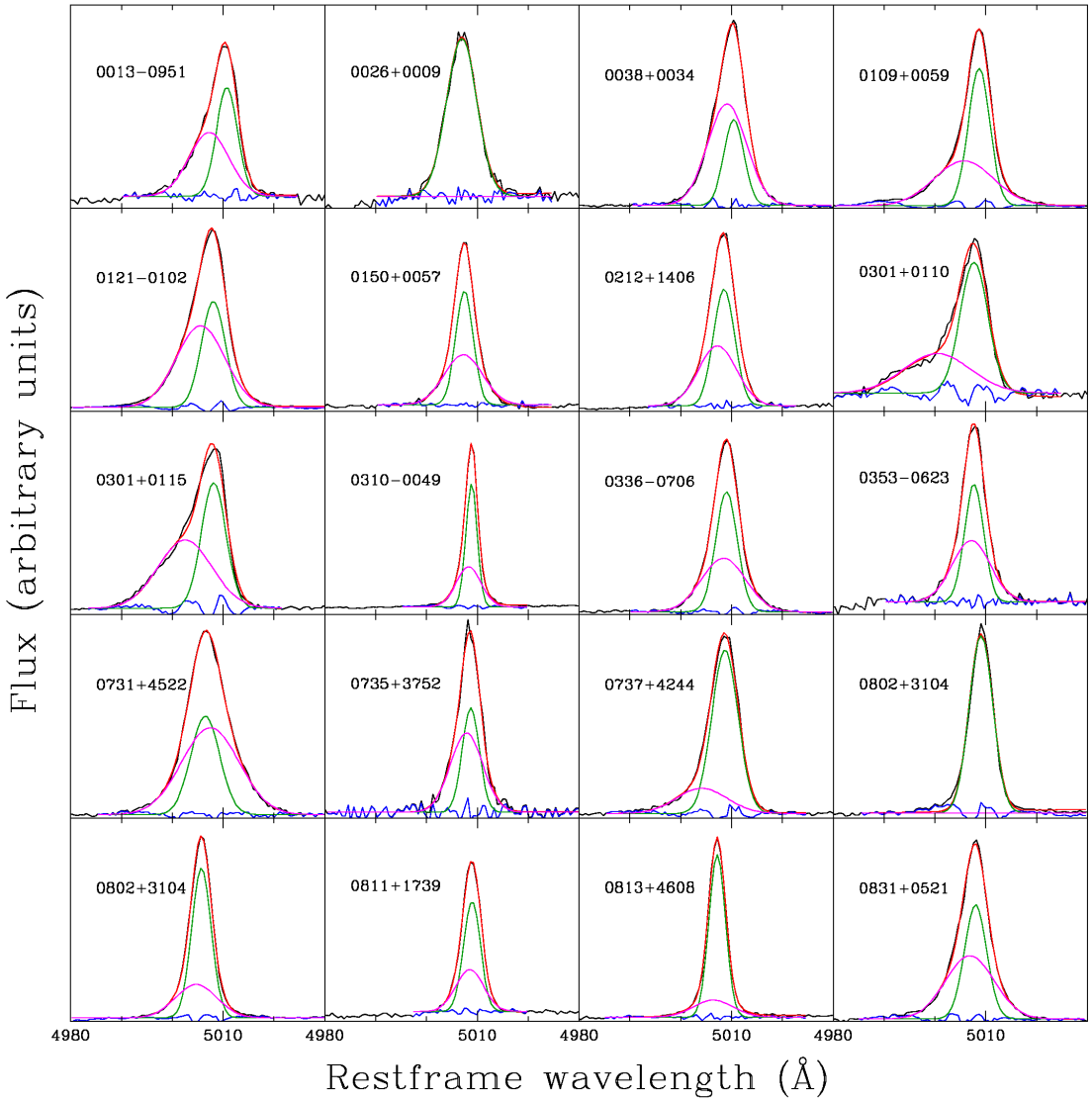

Figure 10: Double-Gaussian [OIII] Fits in RA+DEC Order

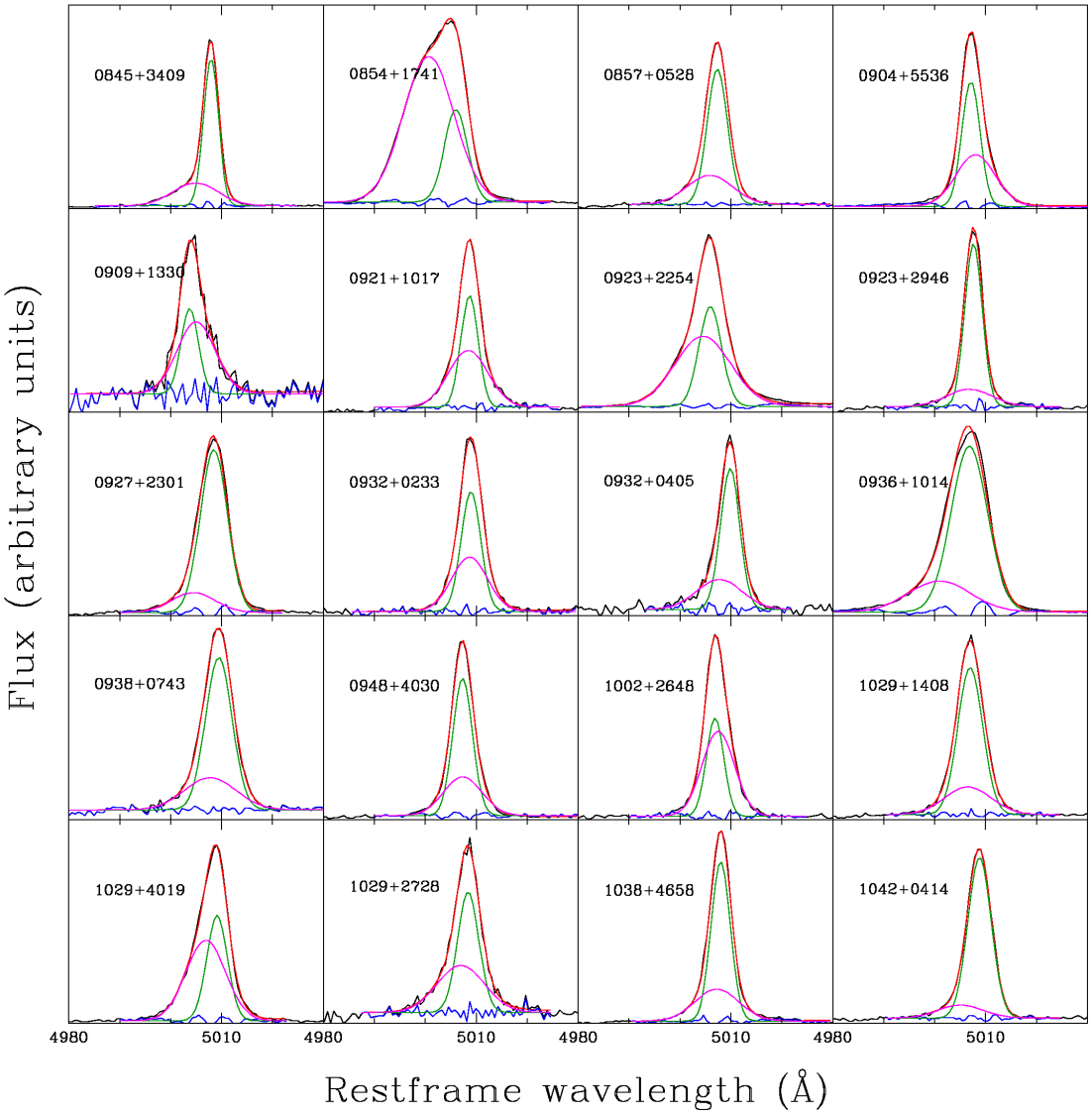

Figure 11: Double-Gaussian [OIII] Fits Continued

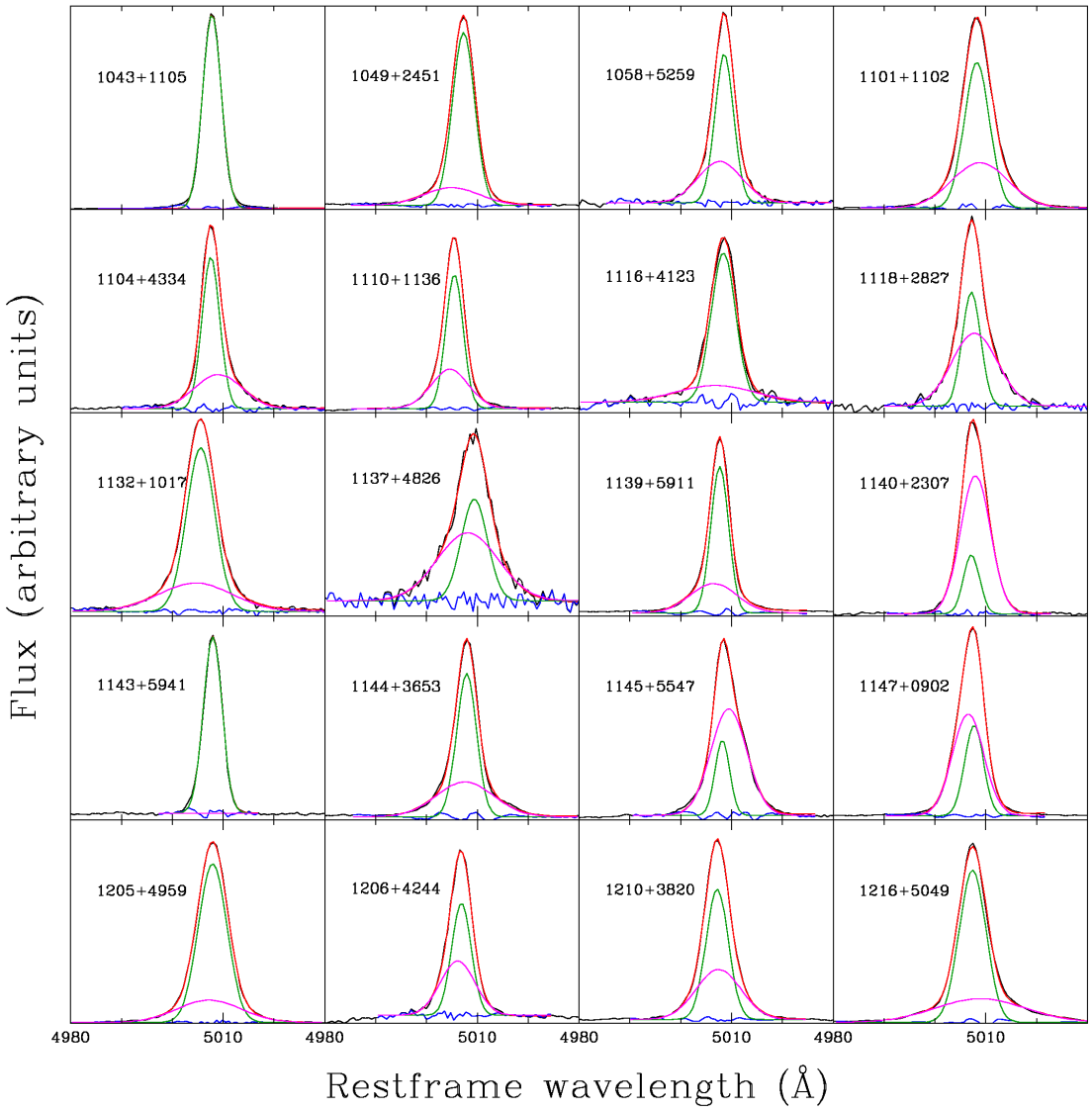

Figure 12: Double-Gaussian [OIII] Fits Continued

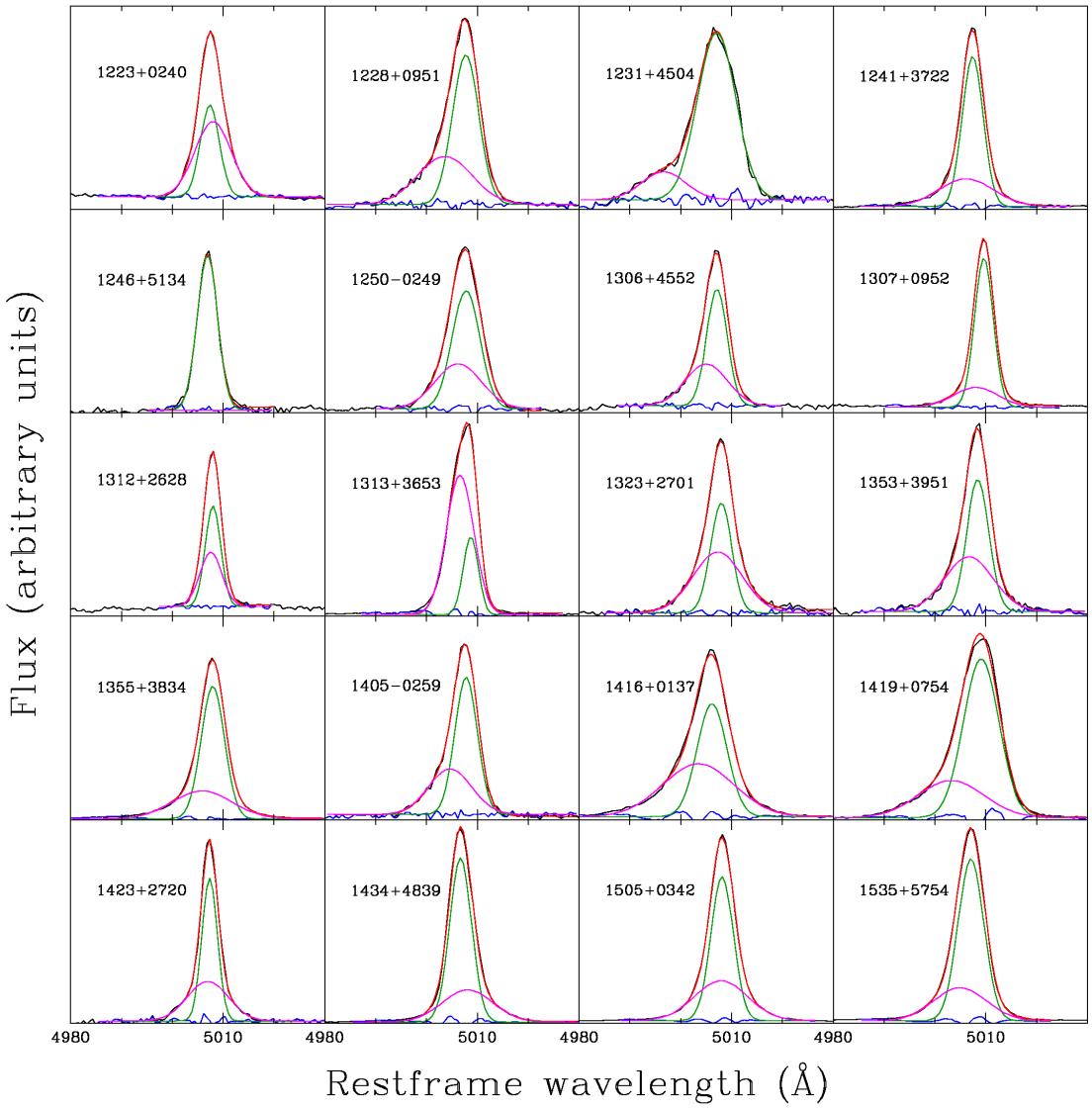

Figure 13: Double-Gaussian [OIII] Fits Continued

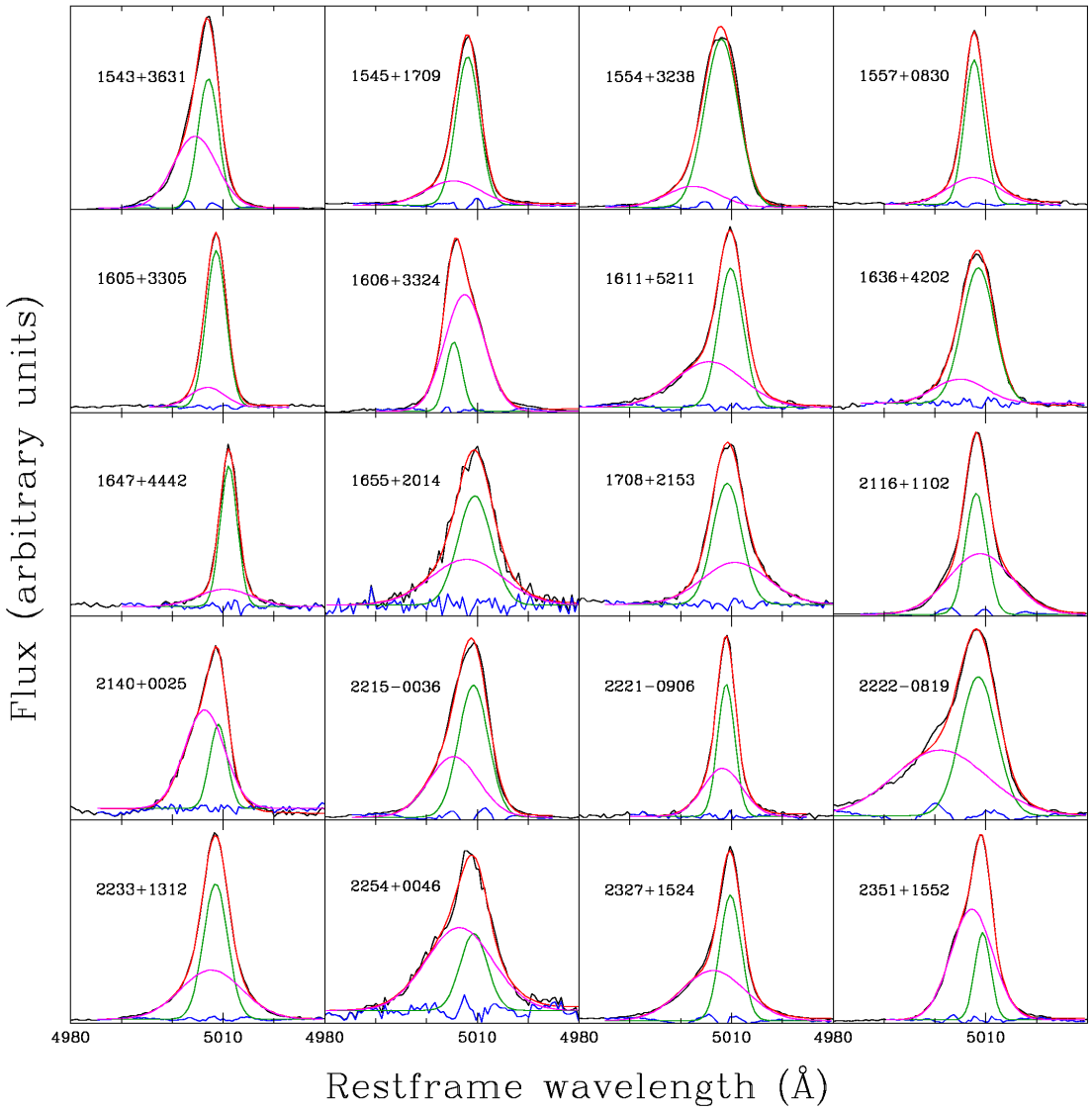

Figure 14: Double-Gaussian [OIII] Fits Continued

Appendix D: Example Python Code

Original code written by Matthew W. Auger. This version modified by Kelsi Flatland, Vardha N. Bennert, and Matthew W. Auger specifically to fit the [OIII] line with two Gaussians in order to account for any outflow wing components.

```
#### Fitting for [OIII] with Wing Component ####
import numpy,pylab,pyfits,sys
import special_functions as sf
from scipy import optimize as optim
from scipy.special import gamma
from mostools import spectools as st

#### THINGS THE USER WILL BE PLAYING WITH ####

## Command-line inputs: ##
# Input arguments go:
# 1(Object Number)
# 2(write or don't write -- y/[n])
# 3(lower fit bound,'lo') 4(upper fit bound,'hi')

# defaults = [object,write?,lo,hi]
defaults = ['00','n',4980,5050]

# Set variables to either their default values or the user-specified value
# first: initialize varlist with the object number
varlist = [sys.argv[1]]
# next: check for whether to write
if (len(sys.argv)>2) and (sys.argv[2]=='y'):
    varlist.append(sys.argv[2])
else:
    varlist.append(defaults[1])
# finally: check other parameters (fit bounds)
for i in range(3,5):
    if (i>len(sys.argv)-1) or (sys.argv[i]=='0'):
        varlist.append(defaults[i-1])
    else:
        varlist.append(int(sys.argv[i]))

# use varlist to initialize these variables
obj,dowrite,lo,hi = varlist
print varlist

# Information for the plots:
```

```
title = '' #title for plot
y1 = -0.1  #flux limits y1 for plot
y2 = 2.5   #flux limits y2 for plot

# Get the full spectrum
filename = 'mbh_subspectra/L%s_sub_mbh.fits'%obj
fullIm = pyfits.open(filename)
wave = st.wavelength(filename,1)
spec = fullIm[1].data.copy()
noise = fullIm[3].data**(0.5)

# Isolate the part of the spectrum that we want to fit
cond = (wave>lo)&(wave<hi)     # places where wave is within our limits
specn = spec[cond]             # spectrum in these limits
waven = wave[cond]             # wavelength in these limits
noisen = noise[cond]           # noise in these limits

# Define the model (for fitting)
def model(parameters,w,s,n,\
          dofit=True,getFit=False):
    # The parameters could change each time
    OiiiLoc1,OiiiWid1,OiiiLoc2,OiiiWid2 = parameters

    # Additional Constrints
    if dofit:
        if OiiiWid1<0.:     # positive width
            return s/n


    # The model is:
    #   first order polynomial 'continuum'
    #   Oiii main line (first Gaussian)
    #   Oiii wing component (second Gaussian)

    #   That's 2+1+1 components
    Model = numpy.empty((4,w.size))

    # First order polynomial continuum
    Model[0] = 0.
    Model[1] = numpy.linspace(0.,1.,Model.shape[1])

    # Oiii main line
    Model[2] = numpy.exp(-0.5*(OiiiLoc1-w)**2/OiiiWid1**2)

    # Oiii wing component
    Model[3] = numpy.exp(-0.5*(OiiiLoc2-w)**2/OiiiWid2**2)
```

```
    lhs = (Model/n).T

    # Create fake data so non-negative is meaningful (ie ensure that the
    #   polynomial coefficients will be greater than 1 by adding a bias)
    data = s+5*Model[0]+5*Model[1]
    rhs = data/n

    # Perform the linear fit to find the weight of each component
    sol,chi = optim.nnls(lhs,rhs)

    sol[:2] -= 5 # Remove the bias from the polynomial weights

    if getFit:
        return (Model.T*sol).T,sol

    if dofit:
        M = (Model.T*sol).sum(1)
        return (M-s)/n

    return (Model.T*sol).sum(1)


# Define the initial guess
zp = 0.           # set continuum to zero, was already subtracted
Oiii1Amp = 9.     # amplitude of Oiii
Oiii1Loc = 5006.85# location of center of Oiii
Oiii1Wid = 5.     # width of Oiii
Oiii2Amp = 3.     # amplitude of wing
Oiii2Loc = 5000.  # location of wing
Oiii2Wid = 10.    # width of wing

pars = [Oiii1Loc,Oiii1Wid,Oiii2Loc,Oiii2Wid]
coeff,ier = optim.leastsq(model,pars,(waven,specn,noisen))

chi2 = (model(coeff,waven,specn,noisen)**2).sum()
print "%5.3f  --  chi^2"%(chi2)

# Get the best fit
fitModel,solution = model(coeff,waven,specn,noisen,getFit=True)


# Calculate flux ratios
flux_nOiii = solution[2]*(2*numpy.pi*coeff[1]**2)**0.5 # Oiii flux
flux_wOiii = solution[3]*(2*numpy.pi*coeff[3]**2)**0.5 # wing flux
flux_Oiii = flux_nOiii+flux_wOiii                      # total flux
```

```
# print ratio of main Oiii to wing
Oiiicb = flux_nOiii/flux_wOiii
print "%5.2f -- flux ratio [OIII]_center/[OIII]_wing"%(Oiiicb)

# print locations of central peak and wing
print "%5.1f -- location of [OIII]_center (Angstroms)"%(coeff[0])
print "%5.1f -- location of [OIII]_wing (Angstroms)"%(coeff[2])

# print sigmas of Oiii and wing
sigmaOiii = (299792*coeff[1]/coeff[0])
sigmaOiiib = (299792*coeff[3]/coeff[2])
print "%5.1f  --  \sigma [OIII]_center (km/s)"%(sigmaOiii)
print "%5.1f  --  \sigma [OIII]_wing (km/s)"%(sigmaOiiib)

# velocity offset
veloffset = (299792*(coeff[2]-coeff[0])/coeff[2])
print "%5.1f  --  velocity offset"%(veloffset)

#### PLOT ####
import pylab
fit = fitModel.sum(0)
diff = specn-fit
pylab.plot(waven,specn,'k') # plots data in black
pylab.plot(waven,fit,'r')   # overplots total fit in red
pylab.plot(waven,diff,'b')  # overplots residual in blue
pylab.xlim(lo,hi)
pylab.title(title)
pylab.ylabel('Flux (arbitrary units)')
pylab.xlabel('Wavelength ($\AA$)')

pylab.figure()
pylab.plot(waven,fit,'k',label='total fit')
pylab.plot(waven,fitModel[2],'g',label='Oiii')
pylab.plot(waven,fitModel[3],'b',label='Oiii_wing')
pylab.xlim(lo,hi)
pylab.title(title)
pylab.ylabel('Flux (arbitrary units)')
pylab.xlabel('Wavelength ($\AA$)')
pylab.legend(loc="upper right")

pylab.show()


#### WRITE ####
```

```
ofile_pref = 'oiiifit_outputDATfiles/%s_'%obj
# Write the data to disk
ofile = ofile_pref+"data.dat"
f = open(ofile,'w')
for i in range(wave.size):
    f.write('%8.3f  %.4e\n'%(wave[i],spec[i]))
f.close()
# Write the fit to disk
ofile = ofile_pref+"fit.dat"
f = open(ofile,'w')
for i in range(waven.size):
    f.write('%8.3f  %.4e\n'%(waven[i],fit[i]))
f.close()
#write the Oiii fit to disk
ofile = ofile_pref+"oiiifit.dat"
f = open(ofile,'w')
for i in range (waven.size):
    f.write('%8.3f  %.4e\n'%(waven[i],fitModel[2,i]))
f.close()
#write the Oiii wing fit to disk
ofile = ofile_pref+"oiiiwingfit.dat"
f = open(ofile,'w')
for i in range(waven.size):
    f.write('%8.3f  %.4e\n'%(waven[i],fitModel[3,i]))
f.close()
# Write the residual to disk
ofile = ofile_pref+"resid.dat"
f = open(ofile,'w')
for i in range(waven.size):
    f.write('%8.3f  %.4e\n'%(waven[i],diff[i]))
f.close()


writefile = open('5007_results.txt','a')
if dowrite == 'y':
    # write all of the relevant output information
    newline = '{0:5}{1:6.2f}{2:8.1f}{3:8.1f}{4:10.1f}{5:10.1f}{6:10.1f}'.format\
              (obj,Oiiicb,coeff[0],coeff[2],sigmaOiii,sigmaOiiib,veloffset)

    newline+= '{0:6}{1:6}   blue'.format\
              (lo,hi)

    writefile.write(newline+"\n")

#### end code ####
```